# Impact Response of Self-Reinforced Polypropylene Sandwich Panels: Numerical Analysis

Sourabh Motiram Gaikwad[1], Sharan Chandran[1]*, Midhun Varma[1], Venkata Sree Harsha[2], Vishnu Vijay Kumar[3]*

[1] School of Mechanical Engineering, Vellore Institute of Technology, Vellore - 632014, India
[2] Mechanical Engineering, SRM University-AP, India-522240
[3] Structural Engineering, Division of Engineering, New York University Abu Dhabi (NYUAD), PO Box 129188 Abu Dhabi, United Arab Emirates

Corresponding author's email: sharanchandra.m@vit.ac.in, vishnu.vijaya@u.nus.edu

**Abstract.** This study introduces a novel self-reinforced sandwich panel design, incorporating a low-density polypropylene (PP) corrugated core between self-reinforced polypropylene (SRPP) face sheets. This structure aims to achieve high energy absorption, good toughness, low density, and full recyclability, addressing key challenges in composite materials for transportation and other industries. Using Abaqus/Explicit, a numerical analysis of the low-velocity impact response was conducted. A nonlinear, 3D finite element model was developed to predict both interlaminar (delamination) and intralaminar (fiber and matrix damage) failure modes, employing Hashin damage criteria and surface-based cohesive behavior. The research demonstrates that damage initiation and appropriate failure criteria can be predicted from the elastic response of the models, offering valuable insights into the performance of these innovative, environmentally friendly sandwich panels under impact conditions.

**Keywords:** Self-reinforced composites, Sandwich panels, Numerical, Polypropylene, Impact response.

## 1 INTRODUCTION

Self-reinforced polypropylene (SRPP) offers several advantages in sandwich panel designs, particularly for impact resistance. SRPP combines high strength with low weight, making it an excellent choice for applications where minimizing weight is crucial, such as in automotive and aerospace industries. SRPP exhibits superior impact resistance due to its ability to deform and absorb energy during an impact, which helps to prevent catastrophic failure. SRPP maintains good ductility, allowing it to flex under stress without breaking. This toughness is essential for absorbing and dissipating impact energy. SRPP is often more affordable than other advanced composite materials, providing a balance between performance and cost. SRPP is resistant to a wide range of chemicals, which enhances its durability in various environments and applications. SRPP can withstand a range of temperatures, making it suitable for applications exposed to varying thermal conditions. SRPP can be produced using recycled materials and is itself recyclable, aligning with growing demands for sustainable materials in construction and manufacturing. SRPP can be easily molded and processed, allowing

© The Author(s) 2025
M. A. Muflikhun et al. (eds.), *Proceedings of the 10th International Conference on Science and Technology (ICST 2024)*, Advances in Engineering Research 268,
https://doi.org/10.2991/978-94-6463-772-4_27

construction and manufacturing. SRPP can be easily molded and processed, allowing for flexibility in design and manufacturing techniques. These advantages make SRPP an attractive option for sandwich panel applications requiring enhanced impact resistance and overall performance.

Impact damage is a significant challenge for composite laminates, particularly in the case of lowenergy impacts that can result in barely visible impact damage (BVID). This type of damage is concerning because it can go undetected during routine maintenance, yet it can substantially reduce a component's residual compressive strength when propagating under normal operating conditions [1, 2]. Advanced non-destructive testing (NDT) methods, such as penetrant-enhanced X-ray radiography and ultrasonic C-scans, are used to identify BVID [3] . The transportation industry has been focusing on improving energy efficiency and reducing fuel consumption to maintain competitiveness. Weight reduction has proven to be an effective method for achieving these goals, leading to increased use of lightweight alloys [4, 5]. However, this approach has also raised production costs. The European Union End-of-life Vehicle Directive 2000/53/EC requires that new vehicles be reusable to a minimum of 95% by weight, driving the development of advanced materials that balance weight reduction, costeffectiveness, and recyclability [6].

Fiber-reinforced polymer (FRP) composites have gained popularity in various industries due to their high specific strength and stiffness [7, 8]. However, they have drawbacks such as low failure strain, brittleness, and complex recycling processes [9]. To address these issues, researchers have turned to self-reinforced composites (SRCs), also known as all-polymer or single-polymer composites. SRCs contain both matrix and reinforcements synthesized from the same thermoplastic family of polymers, offering improved impact resistance and energy absorption [10, 11]. Selfreinforced polypropylene (SRPP) has emerged as a promising material, offering greater toughness, lower cost, and a larger processing temperature range compared to self-reinforced polyethylene (SRPE) [10, 12]. SRPP composites typically exhibit 3 to 5 GPa stiffness, 100 to 150 MPa strength, 15 to 20% failure strain, and superior impact resistance [13]. However, their relatively low stiffness limits their applications in certain fields.

To overcome this limitation, researchers have explored advanced composite structures such as sandwich-structured composites. These structures consist of two thin skins sandwiching a core, providing considerable stiffness and a high strength-to-weight ratio [14, 15]. Various core materials have been studied, including honeycomb structures, foam cores, and corrugated cores [16]. Corrugated core sandwich structures offer several advantages, including high strength-to-weight ratios, resistance to vertical deformation, and improved ventilation to avoid moisture retention [17, 18]. Polypropylene, a thermoplastic polymer known for its ductility and strength at room temperature, has been identified as a suitable material for both the face sheets and core of these sandwich structures [19, 20].

The current study focuses on a novel approach using sandwich panels with self-reinforced polypropylene (SRPP) face sheets and a polypropylene (PP) corrugated core. This configuration aims to achieve a balance between property enhancement and cost-effectiveness while maintaining recyclability. The main objective is to predict the failure mechanisms of these structures under low-velocity impact using finite element analysis. To assess fiber breakage and matrix cracking, the Hashin failure criterion was employed [21]. Core-laminate debonding and delamination among the plies of the face

sheets were accounted for using the surface-based cohesive behavior available in Abaqus/Explicit [22]. The study compared the peak load and energy absorbing capability of SRPP laminated plates with those of the proposed sandwich panels.

Finite element modeling has become an invaluable tool in predicting impact damage and compression after impact (CAI) behavior, reducing the time and cost associated with extensive experimental testing [23]. Previous studies have investigated various aspects of impact damage in composite laminates, including the effects of layup orientations, weave patterns, and stacking sequences [24, 25]. Early research on impact damage growth in laminated plates was limited to simplified layups with few thick layers, making it difficult to differentiate between delamination growth caused by bending cracks and internal shear cracks [26, 27]. More recent studies have incorporated complex interactions between matrix cracks and delaminations of different shapes and sizes [28, 29]. Significant progress has been made in developing finite element models that can accurately predict impact response and damage in composite structures. These models have incorporated various failure mechanisms, including fiber breakage, matrix cracking, delamination, and debonding [30]. The relationship between contact force, penetration energy, and plate thickness has also been extensively studied [31].

## 2 MATERIALS AND METHODS

The material properties of self-reinforced polypropylene (SRPP) are taken from a study performed by Imran Ali et al. [34] and are given in Table 2, in which they used commercially available SRPP sheets under the name CurvTM. These sheets are made of 0/90 woven fabric of polypropylene fibers reinforced in a polypropylene matrix and supplied in preconsolidated form. As the SRPP sheets are made from polypropylene as the base thermoplastic polymer, they are completely recyclable. The compacted thickness of each individual ply is approximately 141 μm. A Hashin damage model is used to observe failure in SRPP laminated plates. Detailed information is given in section 4.1.

The properties of the PP corrugated core are taken from an experimental study performed by Mahmood Shokrieh et al. [35] and are given in Table 2. The yield stress and corresponding plastic strain data are required to define the plastic properties of PP and are calculated per Abaqus documentation. For this purpose, a plot of the engineering/nominal stress versus strain of the PP material is needed. It is taken from a study performed by Mahmood Shokrieh et al. The relationship between the engineering strain and true strain is given by the following equation.

$$\varepsilon_{eng} = \frac{l - l_0}{l_0} = \frac{l}{l_0} - 1 \qquad (1)$$

$$\varepsilon_{true} = \ln(1 + \varepsilon_{eng}) \qquad (2)$$

Now, the relationship between the engineering stress and true stress is

$$\sigma_{true} = \sigma_{eng}(1 + \varepsilon_{eng}) \qquad (3)$$

With the help of the above equations, the true yield stress and true strain are obtained. The strain consists of two components: elastic strain and plastic strain (Figure 1). The

required plastic strain is obtained by subtracting the elastic strain from the total strain. It is represented by the following equation:

$$\varepsilon_p = \varepsilon_t - \varepsilon_e = \varepsilon_t - {}^{\sigma}/_{E} \qquad (4)$$

where $\varepsilon_t$= true total strain,$\varepsilon_e$= true elastic strain
$\varepsilon_p$= true plastic strain, σ = true stress
E = Young's modulus

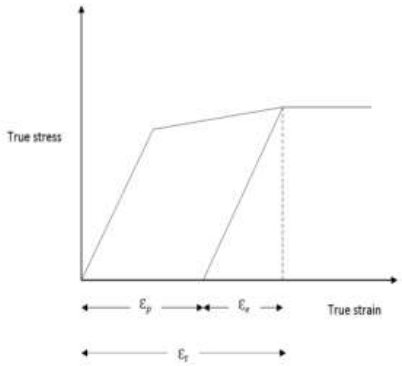


**Fig.1.** Components of true stress/strain

**Table 1.** Mechanical properties of polypropylene

| **Properties** | **Value** |
|---|---|
| Density (kg/m$^3$) | 920 |
| Elastic Properties | |
| E11 (MPa) | 3031 |
| E22 (MPa) | 3031 |
| E33 (MPa) | 1000 |
| G12 (MPa) | 1100 |
| G23 (MPa) | 960 |
| G13 (MPa) | 960 |
| μ12 | 0.23 |
| μ23 | 0.29 |
| μ13 | 0.30 |
| Strength Parameters | |
| Longitudinal tensile strength Xt (MPa) | 141.6 |
| Longitudinal compressive strength Xc (MPa) | 28.56 |
| Transverse tensile strength Yt (MPa) | 141.6 |
| Transverse compressive strength Yc (MPa) | 28.56 |
| Longitudinal shear strength SL (MPa) | 12 |
| Transverse shear strength ST (MPa) | 9 |

**Table 2.** Mechanical properties of polypropylene

| Properties | Value |
|---|---|
| Density (kg/m$^3$) | 910 |
| E (MPa) | 1450 |
| μ | 0.29 |

**Table 3.** Plastic properties of the PP corrugated core

| Yield Stress (MPa) | Plastic Strain |
|---|---|
| 14.64 | 0 |
| 19.196 | 0.009761379 |
| 24.51 | 0.027096552 |
| 28.761 | 0.120164828 |
| 20.471 | 0.211882069 |
| 24.935 | 0.394803448 |
| 34.146 | 0.676451034 |
| 51.955 | 1.064168966 |

The yield stress and corresponding plastic strain data are given in Table 3. The failure mode of the fiber reinforced composite materials was identified via the Hashin damage model [36, 37]. It is considered an important tool for analyzing laminates because it can predict anisotropic damage in fiber-reinforced composite materials and takes into account the failure modes of both the fibers and the matrix in tension and compression. The failure mode of the fiber-reinforced composite.

# 3 DAMAGE MODELING

## 3.1 Hashin Damage

The failure mode of the fiber-reinforced composite materials was identified via the Hashin damage model [36, 37]. It is considered an important tool for analyzing laminates because it can predict anisotropic damage in fiber-reinforced composite materials and takes into account the failure modes of both the fibers and the matrix in tension and compression. The failure ignition criterion can be expressed as Fiber failure in tension: ($\widehat{\sigma_{11}} \geq 0$)

$$F_f^t = \left(\frac{\widehat{\sigma_{11}}}{X_t}\right)^2 + \alpha\left(\frac{\widehat{\tau_{12}}}{S_L}\right)^2 \quad (5)$$

Fiber failure in compression:( $\widehat{\sigma_{11}} < 0$)

$$F_f^c = \left(\frac{\widehat{\sigma_{11}}}{X_c}\right)^2 \quad (6)$$

Matrix failure in tension: ($\widehat{\sigma_{22}} \geq 0$)

$$F_m^t = \left(\frac{\widehat{\sigma_{22}}}{Y_t}\right)^2 + \left(\frac{\widehat{\tau_{12}}}{S_L}\right)^2 \quad (7)$$

Matrix failure in compression:( ($\widehat{\sigma_{22}} < 0$)

$$F_m^c = \left(\frac{\widehat{\sigma_{22}}}{2S_T}\right)^2 + \left[\left(\frac{Y_c}{2S_T}\right)^2 - 1\right]\frac{\widehat{\sigma_{22}}}{Y_c} + \left(\frac{\widehat{\tau_{12}}}{S_L}\right)^2 \quad (8)$$

where
Xt = tensile strength in the longitudinal direction
Xc = compressive strength in the longitudinal direction
Yt = tensile strength in the transverse direction
Yc = compressive strength in the transverse direction
SL = longitudinal shear strength
ST = transverse shear strength
$\alpha$ = a coefficient that denotes the contribution of the shear strength

$\widehat{\sigma_{11}}, \widehat{\sigma_{22}}, \widehat{\tau_{11}}$ = components of the effective stress tensor ($\hat{\sigma}$), which represents the stress acting over the damaged area. The effective stress tensor is calculated from the true stress ($\sigma$) and damage operator (M) as

$$\hat{\sigma} = M\sigma \tag{9}$$

$$M = \begin{bmatrix} \frac{1}{(1-d_f)} & 0 & 0 \\ 0 & \frac{1}{(1-d_m)} & 0 \\ 0 & 0 & \frac{1}{(1-d_s)} \end{bmatrix} \tag{10}$$

This damage operator is equal to the identity matrix before damage initiation. The fiber, matrix and shear damage are characterized by internal damage variables df, dm, and ds, respectively. These internal damage variables are derived from damage variables $d_f^t, d_f^c, d_m^t, d_m^c$ as:

$$d_f = \begin{cases} d_f^t & if \quad \widehat{\sigma_{11}} \geq 0, \\ d_f^c & if \quad \widehat{\sigma_{11}} < 0, \end{cases} \tag{11}$$

$$d_m = \begin{cases} d_m^t & if \quad \widehat{\sigma_{22}} \geq 0, \\ d_m^c & if \quad \widehat{\sigma_{22}} < 0, \end{cases} \tag{12}$$

$$d_s = 1 - (1 - d_f^t)(1 - d_f^c)(1 - d_m^t)(1 - d_m^c) \tag{13}$$

To indicate whether the initiation criterion has been met, an output variable is associated with each initiation criterion, and damage is initiated if its value is 1 or more.

### 3.2 Ductile Damage

The ductile damage model is used as described in Abaqus documentation. This process requires the following properties of polypropylene.

3.2.1 Fracture Strain

The equivalent plastic strain at which damage in a material initiates is the fracture strain. It is calculated by drawing an offset with the same slope of the elasticity modulus of the elastic region, starting from the damage initiation point on the curve and extending to the strain axis.

3.2.2 Stress Triaxiality

The stress triaxiality is defined as

$$\eta = -\frac{p}{q} \tag{14}$$

where p = hydrostatic pressure stress

q = Mises equivalent stress

The hydrostatic pressure stress is one third of the stress tensor trace, and the stress tensor trace is the sum of the principal stresses. This is written in equation form as

$$\eta = -\frac{p}{q} = \frac{\frac{1}{3}\times \text{trace(T)}}{\sigma_{\text{mises}}} = \frac{\frac{1}{3}\times(\sigma_{xx}+\sigma_{yy}+\sigma_{zz})}{\sigma_{\text{mises}}} \qquad (15)$$

The general von Mises stress definition is

$$\sigma_v = \sqrt{\frac{1}{2}[(\sigma_{11}-\sigma_{22})^2+(\sigma_{22}-\sigma_{33})^2+(\sigma_{33}-\sigma_{11})^2]+3(\sigma_{12}^2+\sigma_{23}^2+\sigma_{31}^2)} \qquad (16)$$

3.2.3 Stress Rate

Strain rate, which can be calculated via the following equation:

$$\varepsilon(t) = \frac{L(t)-L_0}{L_0} \qquad (17)$$

$$\dot{\varepsilon}(t) = \frac{d\varepsilon}{dt} = \frac{d}{dt}\left(\frac{L(t)-L_0}{L_0}\right) = \frac{1}{L_0}\frac{dL(t)}{dt} = \frac{v(t)}{L_0} \qquad (18)$$

3.2.4 Fracture Energy

For damage evolution, the energy type damage evolution is specified, which is defined as the energy required for failure after the initiation of damage. Equivalent plastic strain leads to damage initiation, and the area under the curve beyond that value is the fracture energy per unit length. This fracture energy is multiplied by the element characteristic length to obtain the fracture energy, which is used for the damage evolution criterion and can be written as

$$G_f = \int_{\varepsilon_p^0}^{\varepsilon_p^f} l_c\, \sigma_y\, d\varepsilon_p \qquad (19)$$

where the characteristic length can be calculated as

$$l_c = \frac{\text{volume of element}}{\text{area of largest face of element}}$$

The ductile damage evolution properties calculated from the above procedure are given in Table 4.

**Table 4**. Ductile damage evolution properties of the PP corrugated core

| Property | Value |
|---|---|
| Fracture strain | 0.061 |
| Stress Triaxiality | 0.333 |
| Strain rate (1/s) | 6.67e-5 |
| Fracture Energy (N/mm) | 10 |

### 3.3 Surface-Based Cohesive Behaviour

There are various methods for modeling interface behavior, among which cohesive contact behavior is most common. It can be used to model a bonded interface in which the bond may damage and fail as a result of loading. This is an alternative approach for modeling cohesive elements that discretize cohesive materials. The thickness of the adhesive film (PP) needed to bond the laminates and core is negligibly small, and macroscopic properties such as strength and stiffness are not available. Therefore, the

use of cohesive elements to model the response is not appropriate. In this case, a surface based cohesive behavior framework available in Abaqus/Explicit was implemented. Here, the surface interaction property is defined to account for contact cohesive behavior. This contact cohesive behavior is used to model delamination at interfaces, which makes use of the traction-separation law, and it assumes a linear elastic traction-separation law before damage occurs. Progressive degradation of cohesive stiffness is assumed to characterize cohesive bond failure.

In Abaqus documentation, linear elastic behavior is assumed for the traction separation model. It is then followed by damage initiation and evolution. The normal and shear separations along the interface are related to the normal and shear stresses in the elastic constitutive matrix. This represents elastic behavior. The nominal traction stress vector (t) in the elastic– linear softening constitutive model is written as

$$t = \begin{Bmatrix} t_n \\ t_s \\ t_t \end{Bmatrix} = \begin{bmatrix} K_{nn} & 0 & 0 \\ 0 & K_{ss} & K_{st} \\ 0 & 0 & 0 \end{bmatrix} \begin{Bmatrix} \delta_n \\ \delta_s \\ \delta_t \end{Bmatrix} = K\,\delta \qquad (20)$$

where
$t_n$ = normal component of the nominal traction stress vector
$t_s$ = shear components of the nominal traction stress vector
$t_t$ = shear components of the nominal traction stress vector
$\delta_n$ = separation vector components along 3 local directions
$\delta_s$ = separation vector components along the local 1 direction
$\delta_t$ = separation vector components along the local 2 direction

For uncoupled traction separation behavior, $K_{nn}$, $K_{ss}$, and $K_{tt}$ were defined, and the values are listed in Table 5. The failure mechanism includes damage initiation criteria and damage evolution laws. As mentioned previously, the initial response is linear, and after the damage initiation criterion is met, damage occurs according to the damage evolution law specified by the user. Here, the maximum stress criterion is used for damage initiation, which can be represented by the equation below.

$$\max\left\{\frac{t_n}{t_n^0}, \frac{t_s}{t_s^0}, \frac{t_t}{t_t^0}\right\} = 1 \qquad (21)$$

where $t_n^0$, $t_s^0$, $t_t^0$ and are the peak values of the contact stress.
Damage evolution was defined as the energy dissipated because of damage. This energy is the fracture energy and is calculated as the area under the traction separation curve. The surface-based cohesive contact properties are given in the table below.

## 4 NUMERICAL MODEL

In this project, a nonlinear, 3D, finite element model was developed to predict both interlaminar (delamination) and intralaminar (fiber and matrix damage) failure modes with the help of Hashin damage criteria and surface-based cohesive behavior contact properties.

**Table 5.** Surface-based cohesive contact properties of PP

| Property | Value |
|---|---|
| Damage Initiation (Maximum Nominal Stress Criteria) | |
| Normal stress (MPa) | 5 |
| Shear stress 1 (MPa) | 23.1 |
| Shear stress 2 (MPa) | 23.1 |
| Damage Evolution | |
| Fracture Energy (N/mm) | 30 |
| Traction Separation Behavior | |
| Knn (N/mm3) | 137625 |
| Kss (N/mm3) | 52000 |
| Ktt (N/mm3) | 52000 |

### 4.1 CAD Model

The FE model of the laminated plate and sandwich panel is shown in Figure 2. The total size of the laminated plates and corrugated core is 130 mm × 90 mm, and the unsupported size of both models is 125 mm × 75 mm. This is taken from the standard test procedure of the ASTM D7136 drop weight impact testing device [38]. The laminated plate consists of 16 plies of the SRPP, and in the case of the sandwich panel, the top and bottom face sheets contain 8 plies each, resulting in a total of 16. The total thickness of the corrugated core is 5 mm, whereas its wall is 0.4 mm thick. A hemispherical tup with a diameter of 20 mm is modeled, and it is assigned a mass of 1 kg at a reference point. The mass of tup is kept constant for all impact energy levels. In Figure 2(b), the green part represents the PP corrugated core, and the red parts represent the top and bottom face sheets of the SRPP.

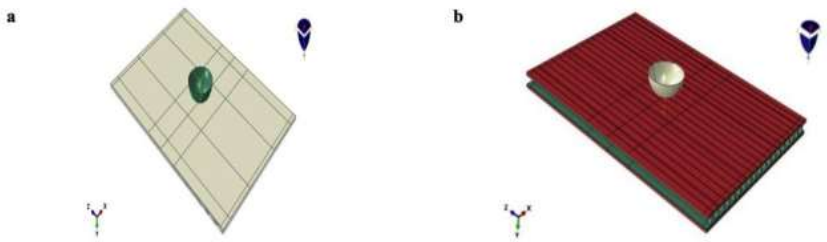


**Fig. 2.** FE model of the (a) laminated plate and (b) sandwich panel

### 4.2 Boundary Conditions

According to [38], the portion of the laminated plate and sandwich panel is fixed by using four lever clamps. This boundary condition is specified by restricting the translational degree of freedom of the edges of the supported portion and leaving the middle portion of 125 mm × 75 mm unsupported. Figure 3 shows the boundary conditions applied over the gray region, and the blue region represents the unsupported

region of the laminated plate and sandwich panel. In the case of hemispherical tup, only vertical translation motion (along the y-axis) is allowed, and the remaining translational and rotational degrees of freedom are restricted. The boundary conditions are represented in Figure 3.

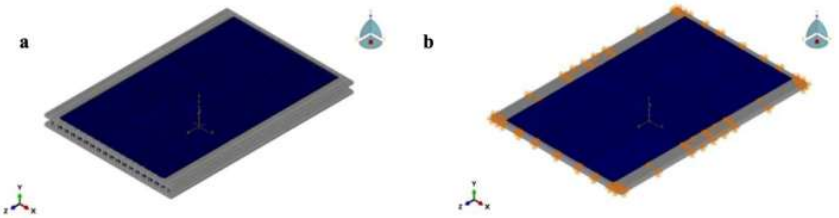


**Fig. 3.** Boundary conditions of the (a) laminated plate and (b) sandwich panel

### 4.3 Load

In this simulation, the model is impacted with energy levels of 16 J, 32 J and 36 J. As the tup is assigned a constant mass of 1 kg, impact energies are obtained by changing either the distance between the tup and top laminate or the velocity of the tup.

### 4.4 Contact Modelling

In this simulation, the model is impacted with energy levels of 16 J, 32 J and 36 J. As the tup is assigned a constant mass of 1 kg, impact energies are obtained by changing either the distance between the tup and top laminate or the velocity of the tup. A general contact algorithm of Abaqus/Explicit is used to define the contact between pairs such as tup-laminate, ply ply, ply core and tup-core. For contact pairs tup-laminate and tup-core, a friction coefficient of 0.3 is used [39].

The surface-based cohesive behavior contact property is assigned to the above pairs, with the exception of tup-laminate and tup-core, to consider the effect of delamination. The properties are given in the table, and a detailed explanation is given in the next section. The output requests, such as displacement versus time and contact force (between the tup and top laminate) versus time, are requested for both laminated plates and the sandwich panel.

### 4.5 Discretization

The laminated plates are discretized with an eight-node general-purpose continuum shell element, with reduced integration with hourglass control (SC8R). SC8R elements resemble 3D elements and allow contact at various surfaces to be specified. Constitutionally, they are the same as conventional shell elements. Therefore, the bending behavior of plies and sub laminates is evaluated better than that of 3D elements and with greater accuracy. The global mesh size is 1.2 mm × 1.2 mm. Eight elements are used in the thickness direction of the laminated plate. In the case of the sandwich panel, face sheets are discretized with the same SC8R elements, and the corrugated core is discretized with an eight-node linear brick element with reduced integration and hourglass control (C3D8R). For the face sheets of the sandwich panel, four elements

per sheet are used throughout the thickness. The smallest edge length of the corrugated core is 0.4 mm. Owing to this, the face sheets and corrugated core are also partitioned such that the mesh at the interface remains the same.

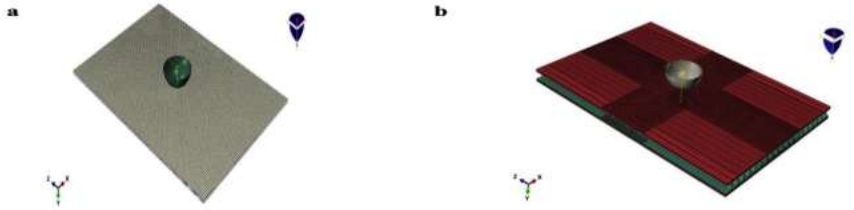


**Fig. 4.** Discretization of the (a) laminated plate and (b) sandwich panel

To reduce the computational cost and obtain uniform results for the sandwich panel, the region near the impact zone is discretized with an element size of 0.42 mm × 0.42 mm, and the global size is increased to 2 mm × 2 mm. The mesh is small enough that the failure load is no longer dependent on the mesh density. Figure 4 shows the meshed models. Furthermore, to reduce the computational time again, mass scaling is performed on elements whose stable time increment is very small and affects the stable time increment of the whole model. While using elements with reduced integration, there are high chances of obtaining spurious energy modes. To suppress this energy, distortion control and enhanced hourglass control are used.

### 4.6 Solver

An explicit code available in the Abaqus solver is used to solve the dynamic loading condition of low-velocity impact. This dynamic explicit step is used for the rapid development of failure. It is also known for analyzing large models with very small dynamic response times, which is required for the models developed in this project. The explicit integration rule is used by the solver to solve such explicit dynamic analysis.

**Table 6.** Peak load and energies

| Type | Peak Load (N) | Energy Absorbed (J) | Damage Dissi pation (J) | Fricional Dissipation (J) | Plastic Dissi pation (J) |
|---|---|---|---|---|---|
| L 16 | 2788.82 | 13.2775 | 1.9926 | 0.0689 | 0 |
| L 32 | 3532.93 | 23.9990 | 4.6766 | 0.1128 | 0 |
| L 36 | 3696.25 | 17.0092 | 15.1073 | 0.3454 | 0 |
| S 16 | 2070.52 | 7.5859 | 1.6609 | 0.0353 | 6.3848 |
| S 32 | 3247.23 | 17.2520 | 5.7274 | 0.0867 | 13.222 |
| S 36 | 3481.879 | 19.4824 | 6.4382 | 0.0981 | 14.9814 |

## 5 Results and Discussions

In numerical analyses of self-reinforced polypropylene (SRPP) sandwich panels using Hashin damage criteria, several failure modes are typically predicted. Each of these modes contributes to the overall failure of the panels in distinct ways. Matrix Tensile Failure occurs when the tensile strength of the polypropylene matrix is exceeded. It can lead to the formation of cracks that propagate through the matrix, reducing the panel's load bearing capacity. Similar to tensile failure, Matrix Compressive Failure happens when compressive stresses exceed the material's strength. This can cause buckling or crushing of the matrix, compromising the integrity of the sandwich structure. Although SRPP primarily involves reinforcement of the matrix itself, any fiber-like structures (if present) can also fail under tensile loading. This failure can reduce the overall stiffness and strength of the panel. Fiber Compressive Failure can occur if the reinforcement fibers experience compressive loads that exceed their limits, leading to localized crushing or buckling. Delamination is a critical failure mode in sandwich structures where the adhesive bond between the face sheets and the core is compromised. Delamination can occur due to impact or shear stresses, leading to loss of structural integrity and load transfer capabilities. Under certain loading conditions, shear stresses can lead to failure within the core material or at the interface between the core and face sheets. This can result in sliding or separation of layers. Each of these failure modes interacts and can exacerbate the others, leading to a cumulative failure of the SRPP sandwich panel. Understanding these modes through Hashin damage criteria helps in designing more resilient panels by optimizing material selection, thickness, and reinforcement strategies to mitigate the impact of these failure mechanisms.

The numerical analysis is focused on failure analysis and prediction of damage under low-velocity impact on a sandwich panel. The numerical simulation is performed for two models: a laminated plate and a sandwich panel. The responses of these two models under three types of impact energies, 16J, 32J and 36J, are recorded. In the case of the SRPP laminated plate, the tup rebounded when impacted with 16 J and 32 J without any visible damage. However, for an impact energy of 36 J, visible damage is first observed at the bottommost ply, after which the tup rebounds. This is shown by the white rectangle in Figure 5(a). In the case of the sandwich panel, for all impact energy levels, the tup rebounds without any visible damage at the bottom face sheet. This is shown in Figure 5(b).

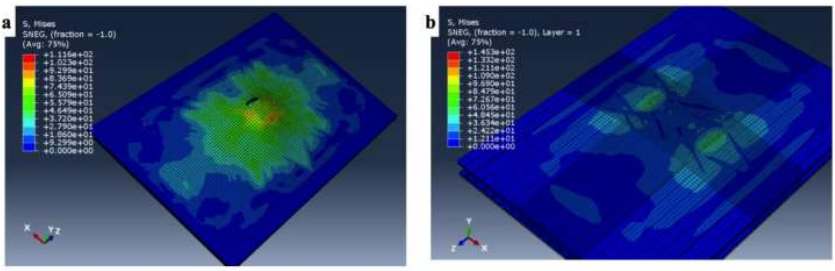


**Fig. 5.** Bottom ply of the (a) laminated plate and (b) sandwich panel

### 5.1 Contact Force and Energy Dissipation

The peak load, energy absorbed and three modes of energy dissipation are obtained through postprocessing and are given in Table 6. The energy absorbed by the model when it is impacted with energy levels of 16 J, 32 J and 36 J is obtained by calculating the area under the contact force vs displacement curve (Figure 8). The configuration naming is performed by mentioning the first letter of the model and is followed by the impact energy level. For example, the first configuration is L16, which corresponds to a laminated plate under an impact energy of 16 J. The last configuration is S36, which denotes the result of the sandwich panel under 36J impact energy.

In the case of the SRPP laminated plate, from the second column of Table 6, the peak load increases gradually when the impact energy increases. A similar trend is observed in the case of the sandwich panel when it is impacted with three different energy levels. If laminated plates and sandwich panels under the same impact energy level are compared, then laminated plates always carry higher peak loads. This is because the force is distributed in the face sheets and the corrugated core of the sandwich panel, which is not the case for laminated plates. The amount of energy absorbed also increases as the impact energy increases, except at L36. Earlier mentioned, damage was visible at the bottom ply of the L36 configuration, which is the reason behind the lower energy absorption (~17 J) than the energy absorption of the previous impact energy level (~24 J) and greater energy dissipation (~15.11 J) at L36. The damage dissipation energy represents the energy that is released through failure modes such as fiber breakage, matrix cracking, delamination between the face sheets and core, and plies within the laminate. These types of failures are more common in L36; therefore, this configuration has a higher damage dissipation energy (~15.11 J) than the other configurations do. The friction between contact pairs, such as tup-laminate and tup-core, represents the total frictional dissipation energy in the model. Friction increased as the impact energy increased, but it was negligible compared to other energy dissipation mechanisms. There is no plastic dissipation of energy in the laminated plate. On the other hand, the polypropylene corrugated core fails through the ductile mode of failure. Most of the energy dissipated by plastic failure of the corrugated core in the case of the sandwich panel, and this energy dissipation increased for 16 J, 32 J and 36 J, respectively. The core allows additional energy dissipation, which adds the advantage of sandwiching a ductile core between self-reinforcement polymers.

### 5.2 Laminate Failure

Fiber damage and matrix damage in the first ply for laminated plates and sandwich panels impacted by 16 J, 32 J and 36 J, as obtained via the Hashin damage criterion, are shown in Figure 5.2. The red color indicates that damage has been initiated. With increasing impact energy, the damage occupies more regions of the sample. In the case of laminated plates, the fiber tensile and matrix tensile failure regions are spread over the entire sample, whereas in the case of sandwich panels (Figure 7), a comparatively smaller region is affected by fiber tensile and matrix tensile failure. This is because more energy dissipates through plastic failure of the corrugated core in the sandwich panels. A similar trend can be seen in the case of fiber compression and matrix

compression failure for all configurations, but the damage region is limited to only the area near the impact region. Among the four damage modes shown in Figure 6 and 7, fiber tensile, matrix tensile and matrix compressive damage occur at ± 450°C.

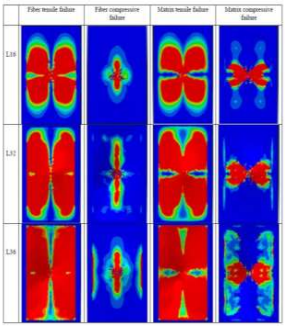

**Fig. 6.** Fiber and matrix damage initiation in the first ply of the SRPP laminated plate

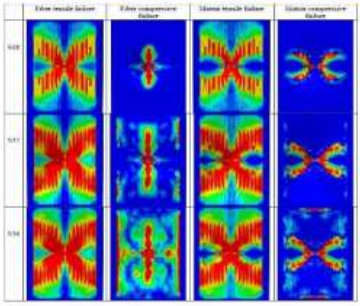

**Fig. 7.** Fiber and matrix damage initiation in the first ply of the sandwich panel

In addition to matrix cracking and fiber breakage, shear cracking is observed for the L36 configuration. This is shown in Figure 8. These types of shear cracks appear because the transverse shear stresses exceed the strength limits. However, shear cracks were not formed in the face sheets of the S36 configuration (Figure 9) because most of the impact energy dissipated in the corrugated core. Furthermore, none of the configurations except L36 satisfied the shear failure initiation criterion for laminates. Figures 8 and 9 show an increase in the damage-prone area over the sample as the impact energy increases in both cases. A comparison of both figures reveals that the damage-prone area is smaller in the case of the sandwich panel. Additionally, the bottom ply of the sandwich panels is safer than that of the laminates. This is the result of the insertion of a corrugated core between the laminates.

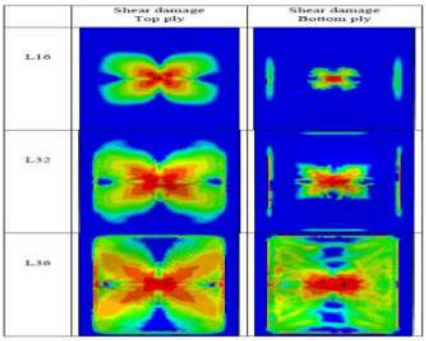


**Fig. 8.** Initiation of shear damage in the top and bottom ply of the SRPP laminated plate

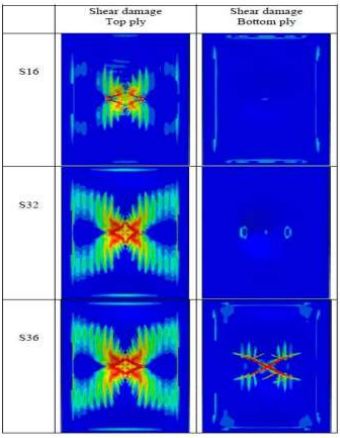


**Fig. 9.** Initiation of shear damage in the top and bottom ply of the sandwich panel

The progression of shear damage when the SRPP laminated plate was subjected to 32 J of impact energy is shown in Figure 11. Ply 1, which was nearer to the tup, experienced greater damage than those plies, which were further away from the contact zone of the tup and top laminate surface. The damage area gradually decreases when moving away from the contact surface. When a corrugated core is inserted between laminates, the damage region decreases drastically. This is shown in Figure 10.

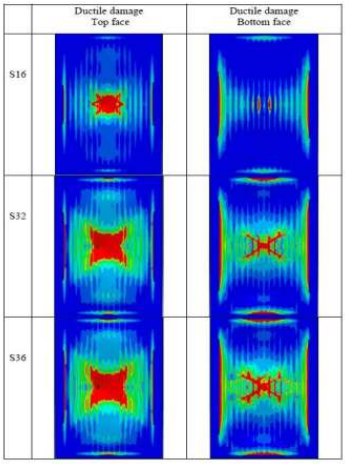


**Fig. 10.** Ductile damage to the top and bottom faces of the PP corrugated core

The discontinuation of shear damage can be observed after eight plies are installed in the top face sheet of the sandwich panel. The corrugated core absorbs most of the impact force, and less force is transmitted to the bottom face sheet. A comparison of both Figure 11 and Figure 12 shows that the damage resistance significantly improves in the case of the sandwich panel. From such contours, we can predict how much of a region is affected for a particular impact energy level.

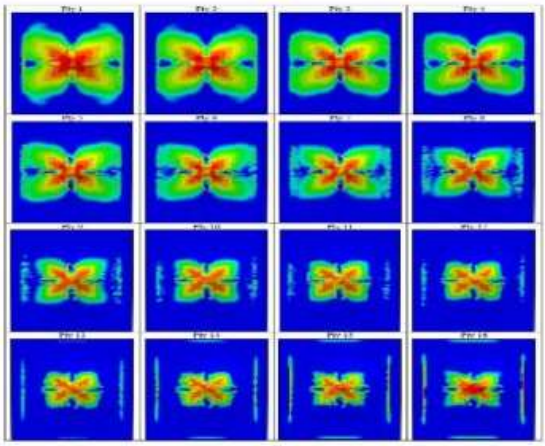

**Fig. 11.** Shear damage in each ply of the SRPP laminated plate under 32 J impact energy

SRPP Laminated Plates typically have good energy absorption due to their homogeneous structure, which allows for uniform distribution of stresses. However,

their ability to absorb energy may plateau at higher energy levels, leading to less effective dissipation beyond certain thresholds. SRPP Sandwich Panels often outperform laminated plates, particularly at higher impact energy levels. The core structure of the sandwich panel provides additional mechanisms for energy dissipation, such as deformation and buckling, which enhance overall energy absorption.

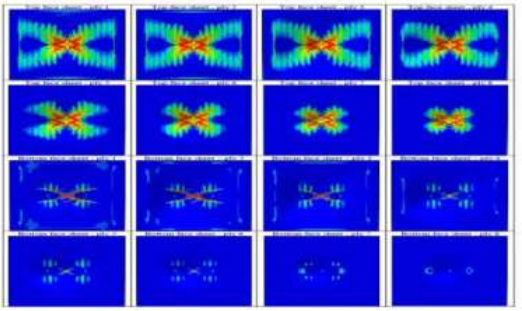

**Fig. 12.** Shear damage in each ply of the sandwich panel under 32 J impact energy

### 5.3 Core Failure

The corrugated core failed through the plastic mode of failure. Figure 5.6 shows the damage area of the corrugated core for both the top and bottom faces. More regions fail when the impact energy increases. All the configurations shown in this figure satisfy the ductile damage initiation criteria. The damage area is concentrated near the impact zone even for the 36 J impact sample. As soon as the tup touches the face sheet, the core starts resisting the impact force and begins to fail when the damage criterion is met. Owing to this, less damage is observed in the face sheets of the sandwich panels, which satisfies the purpose of using a ductile core.

### 5.4 Damage Evolution and Failure Prediction

The impact force history reveals more characteristics of material behavior. The evolution of damage can also be observed from the force–time and force displacement curves. The contact force–time curves of the SRPP laminated plate and sandwich panel for the three impact energy levels are shown in Figure 13. For the laminated plate, the first load drop is observed in the cases of L32 and L36. This is due to initial ply failure, which is not observed at the lowest impact energy level of 16 J (as shown in Figure 13(a) at 1500 N and approximately 0.5×10-3 s). Then, the laminate takes more load, and further loading is supported by subsequent plies. The curve increases until reaching the peak load and then decreases, with linear lines of varying slope. This variation in slope after a tiny interval of time is due to delamination within the plies along with the progressive failure of the plies in the form of matrix cracking and fiber breakage. In the case of L36, all the plies failed, and a small amount of damage was visible.

For the sandwich panel, the curve rises as several lines of varying slope reach the peak load and suddenly drop below. This is shown in Figure 13(b). During this period, delamination occurs several times near the impact zone along with fiber breakage and

matrix cracking, which is why the curve is not smooth. Face sheet failure is the reason behind the first large drop in the curve. After that, the curve rises once again, attains a second peak load and falls continuously because the core is now taking the load and resisting it. During this process, the kinetic energy decreases drastically, and the tup rebounds in the reverse direction.

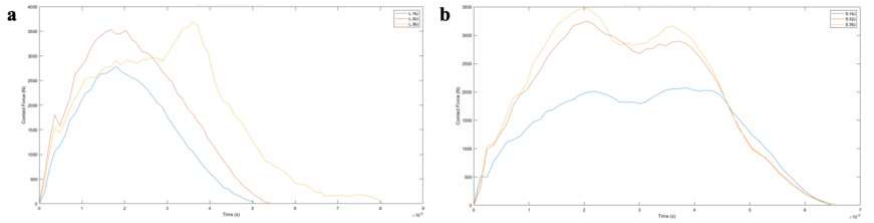


**Fig. 13.** Contact force-time curves of the (a) laminated plate and (b) sandwich panel

The contact force vs. displacement curves of both models for impact energies of 16 J, 32 J and 36 J are shown in Figure 14. After the peak contact force is reached, the tup rebounds.

The reverse path can be seen by the negative path traced by the curve after the peak load is reached. For the case of L36 (Figure 5.10(a)), the curve attains the maximum load and suddenly starts to fall in the negative direction. As mentioned earlier, this behavior is due to failure of the first few plies, resistance of the remaining plies and a reduction in the kinetic energy of the tup. This type of behavior is also observed in all curves of the sandwich panel (Figure 5.10(b)), where in this case, the core resists the motion of the tup just after the load is carried by the face sheet. The curves in Figures 13 and 14 are not smooth because of continuous matrix cracking, fiber breakage and delamination at the ply interface and between the face sheets and core throughout the simulation.

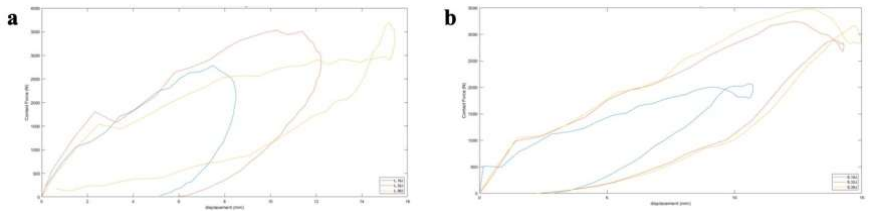


**Fig.14.** Contact force-displacement curves of the (a) laminated plate and (b) sandwich panel

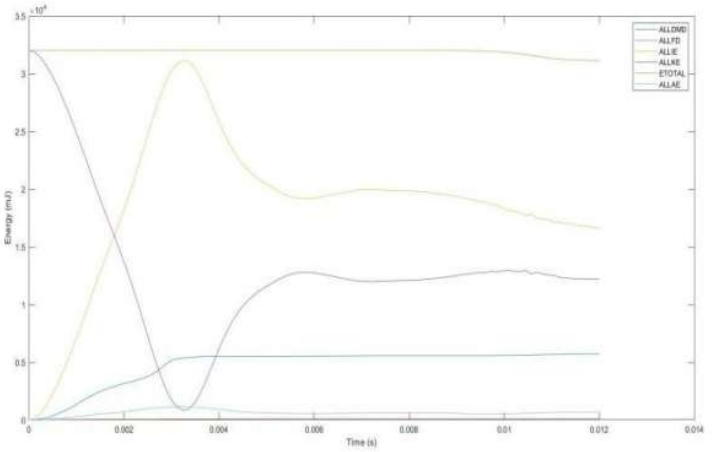


**Fig. 15.** Total energy exchange of S32

The total energy exchange for the model of the sandwich panel under 32 J of impact energy is plotted in Figure 15. The energy associated with all damage modes is repr sented by the ALLDMD curve. The ALLFD represents the energy dissipated through friction and is almost negligible in this case. The curves of total kinetic energy (ALLKE) and total internal energy (ALLIE) nearly mirror each other. The artificial energy or hourglass energy, which is used to remove the hourglass mode, is represented by curve ALLAE. This value is also small compared with the total energy. Finally, the total energy (ETOTAL) in the model is constant throughout the simulation. The total energy and artificial energy curves can be used for quick verification to check whether the numerical model is solved correctly and accurately. If the total energy varies or if the hourglass energy is too high, then the wrong model may be the case, which is not the case for the current model.

The combination of energy absorption, structural integrity, and lightweight properties provided by PP corrugated cores makes SRPP sandwich panels highly effective in resisting low-velocity impacts, thereby enhancing their overall performance in various applications. At 16 J impact, Both SRPP laminated plates and sandwich panels demonstrate effective energy absorption. However, the sandwich panel's core structure may provide slightly better performance due to the enhanced impact resistance from the corrugated or foam core. At 32 J, The performance gap tends to widen, with sandwich panels showing significantly improved energy absorption. The core's ability to deform helps in dissipating energy more effectively than the laminated structure, which may start to experience localized failure. At 36 J, At this higher energy level, the differences are pronounced. SRPP sandwich panels can absorb more energy without catastrophic failure due to their layered construction, whereas laminated plates may suffer from more severe damage, including cracks or delamination. In sandwich panels, energy absorption is aided by multiple failure mechanisms (core deformation, face sheet yielding, etc.), which work together to dissipate energy. In contrast, laminated plates might primarily rely on the matrix and fiber integrity, leading to earlier failure modes under high impact conditions. SRPP sandwich panels generally exhibit superior

energy absorption compared to SRPP laminated plates, especially at higher impact energy levels, making them more suitable for applications where impact resistance is critical.

Surface-based cohesive behavior plays a crucial role in modeling delamination in SRPP sandwich panels during impact simulations. Here are the key aspects of its role. Interface Behavior Representation: Surface-based cohesive behavior models the interactions at the interface between the face sheets and the core material. This allows for the representation of adhesive bonding and the initiation of delamination under stress. The cohesive model includes parameters that define the tensile and shear strength of the interface. It describes how damage evolves as the applied load exceeds these strengths, capturing the gradual degradation of the bond before complete separation occurs. By simulating the cohesive zone, the model can effectively predict how and when cracks initiate and propagate during impact events. This is essential for understanding failure mechanisms and the performance of the sandwich panel under various impact conditions. The cohesive behavior accounts for energy absorption associated with the delamination process. As cracks form and propagate, energy is dissipated, which influences the overall impact response of the sandwich panel. Cohesive models can incorporate nonlinear responses, allowing for realistic simulations of how the material behaves under different loading conditions. This is important for accurately predicting the impact performance and failure modes of the sandwich structure. The cohesive behavior allows for the assessment of the material toughness and adhesion quality, providing insights into how well the panels can withstand impacts and resist delamination. Incorporating surface-based cohesive behavior in impact simulations of SRPP sandwich panels enables a more accurate representation of delamination processes, enhancing the understanding of failure mechanisms and improving the design of more resilient materials.

As impact energy increases, the evolution of matrix cracking, fiber breakage, and shear damage in SRPP laminated plates and sandwich panels follows distinct patterns due to the differences in their structural designs and material configurations. Here's how each damage mode evolves. At lower impact energies, matrix cracking typically initiates first, as the matrix material absorbs initial stress. As energy increases, these cracks can propagate, leading to significant localized damage. The relatively homogeneous structure may allow cracks to spread more easily across the plate. In sandwich panels, matrix cracking may also initiate under lower energy impacts, but the core structure provides additional support. Cracking might be localized due to the face sheets and core absorbing some of the impact energy, which can help limit the extent of matrix damage compared to laminated plates.

Fiber breakage is generally a critical failure mode that becomes prominent as impact energy increases. Once matrix cracking occurs, the load on the fibers increases, leading to tensile failure. As energy levels rise, the likelihood of fiber breakage increases significantly, especially if the matrix can no longer effectively transfer loads to the fibers. In sandwich panels, fiber breakage may be less pronounced initially due to the core's ability to absorb and redistribute energy. However, at high impact energies, if the face sheets experience severe deformation, the fibers may eventually break, especially if the impact results in significant shear forces.

Shear damage can arise due to the lateral forces during impact, leading to sliding between layers or through the matrix. At increasing energy levels, shear damage can

lead to delamination, especially if the matrix has already begun to fail. core structure of sandwich panels introduces additional mechanisms for shear resistance. However, under high impact energy, shear damage can still occur, particularly at the interface between the core and face sheets. Delamination may become critical, where the face sheets separate from the core due to excessive shear forces.

As impact energy increases, both SRPP laminated plates and sandwich panels experience an escalation in damage mechanisms. Laminated Plates Tend to show earlier and more extensive matrix cracking and fiber breakage due to their homogeneous structure, leading to a more rapid degradation of structural integrity. Benefit from the core structure, which helps absorb energy and mitigate damage propagation. However, under high energy impacts, they can still experience significant matrix cracking, fiber breakage, and shear damage, with delamination being a critical failure mode.The progression of these damage modes ultimately informs the design and selection of materials in applications requiring impact resistance.

The use of self-reinforced polypropylene (SRPP) face sheets and polypropylene (PP) corrugated cores in sandwich panels significantly enhances their impact resistance and energy absorption capabilities. Here are the key conclusions: The combination of SRPP face sheets and PP corrugated cores allows for effective energy dissipation during impact. The face sheets can deform under load, while the corrugated core provides additional mechanisms for energy absorption through buckling and deformation, leading to improved overall performance. SRPP face sheets offer a high strength-to weight ratio and excellent toughness, which helps maintain the structural integrity of the sandwich panel under impact conditions. This resilience reduces the likelihood of catastrophic failure and extends the service life of the panels. The corrugated core structure enhances the distribution of loads across the panel. This design helps prevent localized damage and reduces stress concentrations, contributing to a more uniform performance during impacts. The combination of SRPP and PP in sandwich panels can enhance adhesive bonding, thereby reducing the likelihood of delamination, a common failure mode in traditional sandwich structures. This resistance to delamination is critical for maintaining structural integrity after impact.

The materials used—SRPP for the face sheets and PP for the core—are lightweight, making these sandwich panels ideal for applications where weight savings are essential, such as in the automotive and aerospace industries. Given the performance advantages and the relatively lower cost of polypropylene materials, SRPP sandwich panels represent a cost-effective solution for applications requiring high impact resistance. The combination of SRPP face sheets and corrugated PP cores provides design flexibility, allowing for customization based on specific application needs, such as varying thicknesses or core configurations to optimize performance for different impact scenarios. The integration of SRPP face sheets and PP corrugated cores significantly improves the impact resistance and energy absorption of sandwich panels, making them a highly effective choice for applications demanding durability, performance, and lightweight characteristics.

## 6 CONCLUSIONS

SRPP laminated plates and sandwich panels with SRPP face sheets and PP corrugated cores were designed in this project to simulate low-velocity impact events under impact energies of 16 J, 32 J and 36 J and to compare the contact force–time curves, contact force–displacement curves, energy absorptions and peak loads. Hashin damage criteria and surface-based cohesive behavior were used to predict both interlaminar (delamination) and intralaminar (fiber and matrix damage) failure modes. Finally, finite element models of both laminated plates and sandwich panels were established, the impact damage process was analyzed, and the following conclusions were drawn.

1. For both models, a greater impact energy results in a greater contact force and more serious interlaminar and intralaminar damage
2. Under the same impact energy, the contact force of the sandwich panel is less than that of the SRPP laminated plate. This occurred because more impact force was distributed in the PP corrugated core
3. For the SRPP laminated plate, the energy absorption was greater, and as a result, it started to fail at an impact energy of 36 J. On the other hand, the sandwich panel did not experience visible damage at the same impact energy. This occurred because a large amount of impact energy dissipated through the plastic failure of the PP corrugated core. As a result, the proposed SRPP sandwich panel increased the total energy absorption by a factor of 1.18
4. A comparison of the damage profile revealed that the interlaminar damage area in the case of the sandwich panel decreased noticeably because a significant amount of impact energy dissipated in the PP corrugated core
5. A comparison of the results proves that the proposed novel method of using SRPP laminates as face sheets and sandwiching a PP corrugated can be used effectively for lightweight, recyclable applications, such as load-carrying containers, as well as in the marine industry, with improved damage.

## REFERENCES

1. J. Delbeke, A. Runge-Metzger, Y. Slingenberg, and J. Werksman, “The paris agreement,” Towar. a Clim. Eur. Curbing Trend, pp. 24–45, 2019, doi: 10.4324/9789276082569-2.
2. S. Kolluru, A. Thakur, D. Tamakuwala, V.V. Kumar, S. Ramakrishna, S. Chandran, Sustainable recycling of polymers: a comprehensive review, Polymer Bulletin, (2024) 1-42
3. S. Chandran Maniyamparambil, G.K. Vadivel, P. Krishnan, Experimental and numerical damage analysis of low-velocity drop weight impact of polyethylene self reinforced composite laminates for transportation applications, Journal of Thermoplastic Composite Materials, (2022) 08927057221116528
4. R. Smith, Composite defects and their detection, Materials science and engineering, 3 (2009) 103-143
5. V.V. Kumar, D. Narayanan, S. Chandran, S. Rajendran, S. Ramakrishna, Lightweight and sustainable self-reinforced composites, in: Lightweight and Sustainable Composite Materials, Elsevier, 2023, pp. 19-46
6. T.Q. Tran, J.K.Y. Lee, A. Chinnappan, W. Jayathilaka, D. Ji, V.V. Kumar, S. Ramakrishna, Strong, lightweight, and highly conductive CNT/Au/Cu wires from sputtering and electroplating methods, Journal of Materials Science & Technology, 40 (2020) 99-106

7. R. Good, European Union end-of-life vehicles, Envision (DaimlerChrysler internal publication),(September-December), 2 (2000) 4-5
8. V.V. Kumar, S. Rajendran, S. Surendran, S. Ramakrishna, Enhancing the properties of Carbon fiber thermoplastic composite by nanofiber interleaving, in: 2022 IEEE International Conference on Nanoelectronics, Nanophotonics, Nanomaterials, Nanobioscience & Nanotechnology (5NANO), IEEE, 2022, pp. 1-4
9. T.Q. Tran, J.K.Y. Lee, A. Chinnappan, N.H. Loc, L.T. Tran, D. Ji, W. Jayathilaka, V.V. Kumar, S. Ramakrishna, High-performance carbon fiber/gold/copper composite wires for lightweight electrical cables, Journal of Materials Science & Technology, 42 (2020) 46-53
10. V.V. Kumar, S. Rajendran, G. Balaganesan, S. Surendran, A. Selvan, S. Ramakrishna, High velocity impact behavior of Hybrid composite under hydrostatic preload, Journal of Composite Materials, 56 (2022) 3769-3779
11. M.S. Chandran, K. Padmanabhan, A novel correlative formulation of interfacial, quasi-static and dynamic behavior of polyamide self reinforced polymer composites, Materials Today: Proceedings, 46 (2021) 9263-9269
12. P. Krishnan, Self-reinforced polymer composites: the science, engineering and technology, Walter de Gruyter GmbH & Co KG, 2022
13. C. Roiron, E. Lainé, J.-C. Grandidier, N. Garois, C. Vix-Guterl, Correlation between thermomechanical behavior and density of UHMWPE (Ultra-High Molecular Weight PolyEthylene) reinforcements embedded in self-reinforced composites, following a parametric study of the process used, Journal of Polymer Research, 28 (2021) 360
14. C. Gao, L. Yu, H. Liu, L. Chen, Development of self-reinforced polymer composites, Progress in Polymer Science, 37 (2012) 767-780
15. M. Vijayan, V. Selladurai, V.V. Kumar, Investigating the Influence of Nano-Silica on LowVelocity Impact Behavior of Aluminium-Glass Fiber Sandwich Laminate, Silicon, (2023) 1-15
16. A. Kausar, I. Ahmad, S.A. Rakha, M. Eisa, A. Diallo, State-of-the-art of sandwich composite structures: manufacturing—to—high performance applications, Journal of Composites Science, 7 (2023) 102
17. N. Zaid, M. Rejab, N. Mohamed, Sandwich structure based on corrugated-core: a review, in: MATEC web of conferences, EDP Sciences, 2016, pp. 00029
18. B. Han, K. Qin, B. Yu, B. Wang, Q. Zhang, T.J. Lu, Honeycomb–corrugation hybrid as a novel sandwich core for significantly enhanced compressive performance, Materials & Design, 93 (2016) 271-282
19. Q. Ma, M. Rejab, J. Siregar, Z. Guan, A review of the recent trends on core structures and impact response of sandwich panels, Journal of Composite Materials, 55 (2021) 2513-2555
20. B. Du, L.-M. Chen, H. Zhou, Y.-G. Guo, J. Zhang, S.-W. Peng, H.-C. Liu, W.-G. Li, D.-N. Fang, Fabrication and flatwise compression property of glass fiber-reinforced polypropylene corrugated sandwich panel, International Journal of Applied Mechanics, 9 (2017) 1750110
21. B. Alcock, N. Cabrera, N.-M. Barkoula, A. Spoelstra, J. Loos, T. Peijs, The mechanical properties of woven tape all-polypropylene composites, Composites Part A: Applied Science and Manufacturing, 38 (2007) 147-161
22. J. Teckoe, R. Olley, D. Bassett, P. Hine, I. Ward, The morphology of woven polypropylene tapes compacted at temperatures above and below optimum, Journal of materials science, 34 (1999) 2065-2073
23. R. Olley, D. Bassett, P. Hine, I. Ward, Morphology of compacted polyethylene fibres, Journal of materials science, 28 (1993) 1107-1112
24. K.T. Tan, N. Watanabe, Y. Iwahori, Finite element model for compression after impact behaviour of stitched composites, Composites Part B: Engineering, 79 (2015) 53-60

25. V.V. Kumar, S. Rajendran, S. Ramakrishna, Experimental analysis of ballistic impact on carbon, glass and hybrid composite under hydrostatic prestrain, in: Advances in the Analysis and Design of Marine Structures, CRC Press, 2023, pp. 717-721
26. S.N.A. Safri, M.T.H. Sultan, M. Jawaid, K. Jayakrishna, Impact behaviour of hybrid composites for structural applications: A review, Composites Part B: Engineering, 133 (2018) 112-121
27. A.D. Nugraha, V.V. Kumar, J.P. Gautama, A. Wiranata, K.G.H. Mangunkusumo, M.I. Rasyid, R. Dzanzani, M.A. Muflikhun, Investigating the Characteristics of Nano-Graphite Additively Manufactured Using Stereolithography, Polymers, 16 (2024) 1021
28. B. Susanto, V.V. Kumar, L. Sean, M. Handayani, F. Triawan, Y.D. Rahmayanti, H. Ardianto, M.A. Muflikhun, Investigating Microstructural and Mechanical Behavior of DLP-Printed Nickel Microparticle Composites, Journal of Composites Science, 8 (2024) 247
29. R. Mohammadi, M. Assaad, A. Imran, M. Fotouhi, Fractographic analysis of damage mechanisms dominated by delamination in composite laminates: A comprehensive review, Polymer Testing, (2024) 108441
30. B.F. Sørensen, Delamination fracture in composite materials, in: Modeling Damage Fatigue and Failure of Composite Materials, Elsevier, 2024, pp. 221-251
31. Z.-Q. Cheng, H. Liu, W. Tan, Advanced computational modelling of composite materials, Engineering Fracture Mechanics, (2024) 110120
32. G. Wang, W. Jia, F. Cheng, P. Flores, An enhanced contact force model with accurate evaluation of the energy dissipation during contact-impact events in dynamical systems, Applied Mathematical Modelling, 135 (2024) 51-72

**Open Access** This chapter is licensed under the terms of the Creative Commons Attribution-NonCommercial 4.0 International License (http://creativecommons.org/licenses/by-nc/4.0/), which permits any noncommercial use, sharing, adaptation, distribution and reproduction in any medium or format, as long as you give appropriate credit to the original author(s) and the source, provide a link to the Creative Commons license and indicate if changes were made.

The images or other third party material in this chapter are included in the chapter's Creative Commons license, unless indicated otherwise in a credit line to the material. If material is not included in the chapter's Creative Commons license and your intended use is not permitted by statutory regulation or exceeds the permitted use, you will need to obtain permission directly from the copyright holder.